ENGINEERING RESEARCH INSTITUTE
UNIVERSITY OF MICHIGAN
ANN ARBOR

ELECTRON DIFFRACTION INVESTIGATION OF ENGINE WEAR

EXAMINATION OF PISTON RINGS AND CYLINDER BORES RUN IN TEST ENGINES

L. O. BROCKWAY
Professor of Chemistry

and

R. E. ANDERSON
Research Assistant

August 15, 1954

PROJECT NO. 2118
PURCHASE ORDER NO. D 23716

To

ETHYL CORPORATION RESEARCH LABORATORIES
FERNDALE 20
DETROIT, MICHIGAN

TABLE OF CONTENTS

LIST OF TABLES

LIST OF FIGURES

ELECTRON DIFFRACTION INVESTIGATION OF ENGINE WEAR

EXAMINATION OF PISTON RINGS AND CYLINDER BORES RUN IN TEST ENGINES

I. INTRODUCTION

This study was undertaken to test the applicability of electron diffraction methods to the examination of piston rings and cylinder bores run in test engines. The tests run by the Ethyl Corporation were adjusted to determine the effect of various fuel additives on wear and surface conditions in the engine. The examination by diffraction methods should provide information on the chemical and physical changes occurring on the surfaces during running; in particular, the results should indicate the occurrence, distribution and orientation of crystalline phases such as graphite, iron oxides and other possible products of chemical attack and deposit. The correlation of this information with other test data such as engine speed, load, type of fuel and lubricant, observed wear rates and metallographic changes occurring beneath the surfaces should contribute to a fundamental understanding of the wear processes in reciprocating engines.

The use of electrons for diffraction in contrast with X-radiation provides diffraction patterns characteristic of the surface layer less than 10^{-6} cm. thick in favorable cases and thus permits the identification of extremely minute quantities of material spread over a surface or formed in the early stages of a corrosive chemical attack on the surface. Supplementary information on the deeper layers may be supplied by X-rays and the two methods are useful in conjunction. The use of electrons in the microscopic examination of surface replicas should also be noted as valuable in studying the distribution of surface phases.

Previous examination of engine surfaces by electron diffraction techniques have been reported by Finch, Quarrel and Wilman (Trans. Faraday Soc. (London), Vol. 31, pp. 1051-1080, 1935) and by Brockway and Nowick

(NACA Report No. E76, 1945) but both reports cover tests on aircraft engines for which the operating conditions are not specified in detail and where no correlation with wear rates was attempted.

The present examinations were carried out on specimens from engine tests using various fuels, including a standard clear fuel (no additive), and the standard fuel plus tetraethyl lead with and without halides, and the standard plus iron carbonyl with and without a zinc compound. The details of these specimens and their results are given below following a description of the electron diffraction method. Some preliminary work was also done with replicas in an electron microscope.

II. THE ELECTRON DIFFRACTION METHOD

Diffraction technique. The electron diffraction examination is made by directing a narrow beam of monoenergetic electrons at a glancing angle onto the surface of the specimen and recording the scattered electrons photographically. The equipment used here is an RCA EMD-2 unit producing 50,000-volt electrons with a beam width of about 0.5 mm. at the position of the sample. The sample-to-photographic-plate distance is roughly 50 cm. An auxiliary electron gun can be used to bathe the sample in high intensity low voltage electrons for neutralizing the charge sometimes accumulated from the main electron beam on a non-conducting surface layer of the specimen. For each exposure a specimen of no more than three quarters of an inch in any dimension is mounted roughly parallel to the beam and the angle to the beam is adjusted until the pattern appears favorable on the fluorescent screen, and an exposure of about a half a minute is made on a photographic plate. The 4" x 5" photographic plates (Kodak Process) are developed for maximum contrast in Kodak D-11 for four minutes, and fixed in Kodak F-5 for about twenty minutes.

The patterns obtained from a surface covered with a randomly oriented microcrystalline material show the concentric arcs analogous to X-ray powder diffraction patterns. The ring spacings are measured and computed in terms of the crystallographic interplanar distances (Bragg "d" values), and for identification purposes these are compared with the X-ray patterns of known materials (especially as found in the A.S.T.M. File of Powder Diffraction Patterns) or with standard electron diffraction patterns prepared from known specimens. The measured d values are calibrated with the aid of transmission patterns of zinc oxide, which gives many sharp rings of known d values..

In all of the diffraction work on engine surfaces the "reflection" technique was used with the electron beam striking the surface at an angle of 1° or 2°. Patterns of this type (illustrated for graphite and two iron oxides in Figure 3) show semi-circles whose radii are measured for computing the Bragg d values. Two principal uncertainties occur: (1) that in determining the position of any one diffraction ring which in reflection often tends to be

more diffuse than in transmission patterns, and (2) the possible displacement of the unscattered beam due to charging effects on the specimen. In favorable cases (i.e., rings not too diffuse and showing in good contrast against the background of inelastic scattering) the precision of the d values below 1.50 Å is about 1%; higher d values corresponding to smaller diffraction rings show less precision. Plates suspected of showing a displacement of the main beam can sometimes be measured with reference to a center determined from the arcs rather than from the mark of the beam on the emulsion.

The intensities of the rings are visually estimated and graded on a qualitative scale running from strong through medium, weak and very weak. The relative intensities are also compared between the unknown and standard patterns in making an identification.

Specimen Preparation. The specimens received from the Company (see Table IV) were all taken from test runs designated 52G1-A0 through 52G1-A21 made on a test engine operated in the Company laboratory. The engine was an Ethyl designed single cylinder 1951 Oldsmobile type with wet liner. The C.F.R. high-speed crankcase was coupled to a synchronous motor. The piston assembly included the standard Oldsmobile aluminum piston with widened (.1260") top groove, .1245 - .1250" cast iron flat face top compression ring supplied by the Perfect Circle Co., and the ordinary Oldsmobile second compression and oil rings. Bore: 3 3/4". Stroke: 3 1/4".

In the usual procedure the engine was dismantled immediately following shut down, and the piston rings and cylinder liner were cleaned in kerosene and coated with grease to reduce atmospheric corrosion. The top piston ring was cut in six equal segments and three alternating segments (a, c, e) were submitted for electron diffraction examination. The cylinder liner was cut in longitudinal segments, and four strips (a, c, e, g) 1/4" wide and located at 90° positions around the cylinder were submitted.

Preparation of the specimens for electron examination started with a twenty-minute wash in toluene to remove the protective grease. From a ring segment a specimen 3/4" long was cut, washed in toluene for several minutes more, fastened in the demountable specimen holder of the diffraction unit,

washed for forty minutes in specially purified benzene in a Soxhlet extractor, and then mounted in the diffraction unit which was immediately evacuated. The exposure to air was never more than a few minutes. Certain specimens were abraded lightly on 3/0 emery just before mounting in the diffraction camera.

Specimens from the cylinder liner (see Figure 1) were taken by cutting the 1/4" strip at the following distances from the top of the cylinder: 3/16", 1/2", 1", 2", 3 1/2" and 5"; they were designated in order by Roman numerals; thus the specimen A2eII was the 5/16" piece found between 3/16" and 1/2" of the cylinder top and lying in quandrant "e" of the cylinder liner taken from test run A2. A2eIV was a 1/2" piece above the 2" cut. In this engine, the upper edge of the top compression ring at top dead center is 7/32" from the top of the cylinder. At bottom dead center, the lower edge of the oil ring is 4 1/8" from the cylinder top. Cylinder liner specimens were washed and mounted in the same way described for ring specimens.

Interpretation of Diffraction Patterns. Because the electron beam has a limited penetration, the diffraction patterns arise mainly from material on the surface, with very little contribution from the underlying matrix phase. Furthermore, the strong scattering power of material for electrons (about 10^6 times that for X-rays) makes it possible to obtain good patterns from very small quantities of material. For identification, comparison of the measured d values can often be made with the X-ray data of the A.S.T.M. tables but the discrepancies in the relative intensities due to the greater absorption of electrons may be confusing. It may also be noted that X-ray data obtained at large scattering angles is more precise than the electron data and the discrepancies of 1% or more in the d values may also be confusing. For these reasons standard patterns prepared by the same technique used for the unknown material are advantageous.

Standard diffraction patterns were prepared of α-Fe, graphite, α-Fe_2O_3 and γ-$Fe_2O_3 \cdot H_2O$. The iron pattern was obtained from a low-carbon rolled steel after light abrasion with 2/0 emery. The graphite pattern was taken from a smear on a metal plate of a graphite suspension in water. The α-Fe_2O_3 pattern was given by a low-carbon steel which was etched with dilute nitric acid and then heated in air until blue interference colors appeared. The γ-$Fe_2O_3 \cdot H_2O$ is the structure produced by the corrosion of iron in a

moist atmosphere; a thick layer was produced by suspending a piece of cast iron above water at 50°C for twenty-four hours.

The identification by comparison of d values and intensities is shown for a typical pattern in Table V where the results of this study are presented. Certain special problems in identification are discussed in the following paragraphs.

The oxides, α-Fe_2O_3 and Fe_3O_4, have been found to occur together on ring and bore surfaces. Although these oxides crystallize in different structures, the patterns show a pronounced similarity requiring special care in making the identification as illustrated in Table I for a typical oxide pattern. Strong distinguishing lines do occur at 2.71 and 1.85 Å in the case of α-Fe_2O_3 and 2.97 and 2.42 Å in the case of Fe_3O_4. Wherever lines in diffraction patterns have occurred indicating any iron oxide, a careful examination has been made for these distinctive lines. The existence of γ-Fe_2O_3 should also be noted; its structure is so near that of Fe_3O_4 that they cannot be distinguished by diffraction patterns. For this structure the composition corresponding to Fe_3O_4 is the more usual, and the "Fe_3O_4" designation is used in this report.

A further possibility exists in the case of engine tests involving a fuel or oil additive containing zinc compounds. The spinel-type compound, $ZnFe_2O_4$, has a structure identical to that with Fe_3O_4 (i.e., with Zn replacing one of the Fe atoms), and because the cell edges of the crystals are very nearly the same in length these two compounds are indistinguishable by diffraction tests. It may be noted that the possibility of the occurrence of such a spinel-type compound involving an element from fuel or oil additives could be readily tested if cadmium were used in place of zinc in the additive, since the cell size of the cadmium spinel is quite different from that of Fe_3O_4. Table II shows the close similarity between d values and relative intensities of the spinel type structures of Fe_3O_4 and $ZnFe_2O_4$, and the differences in the case of $CdFe_2O_4$.

The substances whose occurrence was considered to have some probability in various tests and whose patterns were compared with all unknowns include the following: α-Fe, graphite, Fe_3O_4, α-Fe_2O_3, γ-Fe_2O_3, α-$Fe_2O_3 \cdot H_2O$, β-$Fe_2O_3 \cdot H_2O$, γ-$Fe_2O_3 \cdot H_2O$, α-Al_2O_3, Sn and SnO_2. In addition, a series

of lead compounds were considered as listed in Table III, for most of which the diffraction data were supplied by the Company.

Some patterns show discontinuities in the diffraction rings indicating non-random orientation or a limited number of crystallites of the corresponding phase. In the tables of results this is indicated by a single or double asterisk.

Estimates of Relative Amounts. After the phases have been identified on each ring and bore specimen a rough estimate is given of the relative amounts of graphite and iron oxides, using a scale ranging from vs (very strong) to vw (very weak). Estimates of good precision are not possible because most of these patterns show a higher background of diffuse scattering than is given by surfaces specially prepared for electron diffraction examination. Typical good patterns are shown in Figure 2 for ZnO (transmission) and α-Fe_2O_3 (reflection). Some of the better patterns from ring and bore specimens are shown in Figure 3, but most of them show even more background relative to the diffraction rings.

In the tables of results discussed in the next section the relative amounts of the different phases are indicated but it must be emphasized that the comparison is much more reliable for different phases in the same pattern than it is for the same phase in different patterns. The intensities and resolutions in patterns from different specimens are influenced by several factors (the roughness of the surfaces, the actual location of the crystallites of a given phase in relation to surface asperities, the orientation of the electron beam relative to surface features, and the total electron exposure reaching the several phases). For this reason the comparison of the amounts of phases in a pair of patterns is to be made only with extreme caution. The estimates given in Table IV of the relative amounts of phases appearing on the top piston rings in different runs represent the best judgment of the investigators based on all of the exposures from one piston ring (as indicated in the preceding column of Table IV).

The results for different areas on the same ring show some variation, but this is to be expected since the spreading of graphite from inclusions

in the cast-iron, the oxidation of the iron, and the loss of material by abrasion can hardly be completely uniform over the surface of the piston ring.

III. RESULTS AND CONCLUSIONS

The specimens of top rings received from the Company are listed in Table IV together with the test conditions and a summary of the electron diffraction results. Three main fuel conditions were used: (1) clear fuel, (2) with TEL additive, and (3) with iron carbonyl additive. The results are grouped below to show comparisons between the clear fuel and the two classes of additive.

The direct diffraction results are illustrated by the prints of selected patterns in Figure 3 and by the comparison in Table V between the d values measured in a typical mixed oxide pattern (A12c) and those for the standard patterns. Examination of the original negative and of the data in Table V lead to the conclusion that this pattern is due to weak graphite and strong oxides (α-Fe_2O_3 + Fe_3O_4) with no real evidence for a predominance of one oxide over the other. Information of this kind is given in Tables VI, VII and IX for each ring segment which gave any electron diffraction pattern. Similar results appear in Table VIII for the cylinder bores.

Runs with Leaded Fuels: Ring Specimens. Ring specimens were examined from runs in which neat TEL was the additive (A5) and with TEL plus halides as 62-MIX (A3, A6, A18, A19). These runs are compared with runs where clear fuel was used (A20 and A21) and clear fuel with a zinc oil additive (A4). Results of the phases found on the individual specimens when leaded fuels are used are given in Table VII, with a scale of letters which gives a qualitative estimate of the relative amounts of the phases. Table VI gives the results when clear fuels are used. Among these runs only two provide any test of reproducibility: A6 and A18 used the same additive and engine operation speeds and very nearly the same total running time. All the other runs show appreciable variation in some of the factors. A summary of these results together with weight loss data is given in Table IV.

The phases identified are the same in all of these runs, i.e., graphite, α-Fe_2O_3, and Fe_3O_4, with the exception of A5 where δ'-$Fe_2O_3 \cdot H_2O$ was found, but the relative amounts of these phases appearing on these ring surfaces differ greatly among the runs.

It may be emphasized here that no lead compounds have been detected on the faces of the top rings of these runs as examined in the electron diffraction tests. Because of the interest in this point arising in connection with the use of leaded fuels a careful examination was made for the occurrence of any diffraction rings which might be attributed to the lead compounds listed in Table II. In no case is there any evidence for any of these compounds.

Because of the possibility in some cases that the more abundant graphite might be covering the oxide, some of the specimens were abraded lightly with 3/0 emery; this treatment disturbs enough of the surface sufficiently that all phases at or near the surface are made available to the electron beam. Abrasion caused the α-Fe pattern to appear but in no case was the oxide pattern made appreciably stronger.

The summary in Table IV indicates that when clear fuel is used there is an increase in the amount of graphite present from the short to the long run (16 and 81 hours) and there is also an increase in the amount of oxide. The run with neat TEL shows strong graphite and weak oxide, a condition which is similar to that observed for the run with clear fuel with an oil additive.

A3 and A6 were both run with the 62-MIX as the additive for roughly the same length of time, although a difference in the engine speed was reported. It is interesting to note that in A3 the diffraction rings are continuous showing a completely random orientation of the graphite flakes, while on A6 the graphite flakes show a tendency toward preferred orientation. The specimens abraded with 3/0 emery always show random orientation of graphite, which leads to the suggestion that any action opening up graphite inclusions in the cast-iron but not followed by a milder rubbing action will show randomly arranged particles of graphite. In this respect the high wear rate of run A19 (117 mgm. weight loss in 16 hours) may be contrasted with that of run A11 (792 mgm. in 92 hours); the former shows orientation in the graphite while the latter does not.

A fuel with TEL plus halides gives predominating graphite in two cases and predominating oxide in the other two. The duplicate runs (A6 and A18) are reversed in this respect, indicating that the reproducibility between runs is not very good as tested by the relative amounts of phases appearing on selected areas of faces of the top rings. Different segments of the same ring give the same qualitative results but the reproducibility between runs is not as good. This lack of reproducibility is especially noticeable in the wear rate (Table IV) observed for runs A18 and A19. The total wear measured by the weight loss of the top ring amounted to 52 mgm. in the first run of 81 hours and 117 mgm. in the latter run of 16 hours. It is noteworthy here that the very high wear rate observed in run A19 is accompanied by the strongest iron oxide pattern found in any runs considered in this section.

The following conclusions may be noted:

With the use of clear and leaded fuels the face of the top ring is covered with graphite, α-Fe_2O_3, and Fe_3O_4.

No lead compounds of any kind have been detected on the faces of the rings in runs using leaded fuels.

The reproducibility of the runs is open to question since the only pair of duplicate runs (A6 and A18) show weight losses of 23 and 52 mgm. respectively and the reversal of the relative amounts of graphite and iron oxide.

In all of the runs with clear and leaded fuels there appears to be some correlation between total wear and the total amount of oxide. The three runs with lowest wear (A20, A6 and 5 ranging from 4 to 26 mgm.) all show weak oxide; the next three (A21, A3 and A18 ranging from 37 to 52 mgm.) show medium oxide in two cases and weak in the third; the run with the highest wear (A19 at 117 mgm.) shows medium strong oxide. The difficulty of comparing the amounts of a single phase in the patterns from different specimens may again be noted, but because of the care in examining these specimens under the same conditions the comparison made here has some validity. The total oxide is evidently not related to the duration of the run (or the average wear rate) since the least and the greatest total wear both occurred in sixteen hours while all the other runs were much longer (seventy-five to ninety-nine hours).

Among these same runs the relative amounts of oxides and graphite on a given ring indicate a predominance of oxide in the two short runs (A20 and A19). Three of the five long runs show a clear predominance of graphite, one shows predominant oxide and the other is uncertain.

Finally, the data available here do not show any clear distinction between the use of leaded and non-leaded fuels.

Runs with Leaded Fuels: Cylinder specimens. Cylinder liner specimens were examined at different positions along the cylinder as located in Figure 1, and the results are shown in Table VIII. Preliminary work on two runs, A2 and A4, estabilshed the striking result that at the top of the piston travel strong oxide patterns are found which diminish down the length of the cylinder and disappear at the bottom. The graphite distribution was found to be just the reverse, light at the top and heavy at the bottom. No completely random graphite pattern was obtained here, an indication that the cylinder wall is not disturbed as deeply as the ring surfaces. One exceptional case, A2e, is included in the table; it shows the opposite directions for distribution of oxide and graphite.

Additional work on bore specimens from run A4 clarified the nature of the oxide. Sections cut from the bore segment A4e show once again that iron oxide predominates near the top of the ring travel and becomes weaker at the bottom whereas graphite is weaker at the top and predominates near the bottom; but because the diffraction patterns from the bore segments are sharper and better resolved than those from piston ring segments, the comparison of the spinel-type oxide (Fe_3O_4) with the α-Fe_2O_3 is more reliable here. The amount of Fe_3O_4 is definitely larger than the amount of α-Fe_2O_3 on these cylinder segments. It is possible that this spinel structure contains zinc (since the oil additive in this run contains zinc) but as mentioned before it could not be distinguished from Fe_3O_4. For testing its effect on the cylinder wall the use of a cadmium additive would be interesting to allow a clear distinction between the cadmium spinel and the Fe_3O_4 phase. The data indicate in the case of the A4 segment a high degree of preferred orientation in both the graphite and iron oxide phases.

Diffraction work on run A5 indicated that the only iron oxide phase observed on the bore segments is γ-$Fe_2O_3 \cdot H_2O$. Since this corresponds to the phase produced in normal rusting in a moist atmosphere, it is probable that this specimen was not sufficiently protected from the atmosphere prior to its examination; but the predominance of this phase near the top of the ring travel with falling off down the cylinder follows the behavior of the other oxides observed on other cylinders. The usual increase in graphite down the cylinder is observed here.

In a comparison of the results with different fuels it is noted that in most of the specimens from runs A18 and A19 (62-MIX) the directions of the distribution of oxides and graphite differ from that of run A4 (no fuel additive, but oil additives). Specimens A18a and A19a show strong graphite at both the top and the bottom of the ring travel, and the distribution of oxide is the reverse of that in run A4. Allowing for some variations, the same general trend for the distribution of graphite is observed in runs A20 and A21 (clear fuel) as in run A4. The latter shows a diminution in the amount of oxide down the region of the ring travel whereas the amount of oxide changes very little from segment to segment in runs A20 and A21. In runs A21e II and IV the amounts of Fe_3O_4 and α-Fe_2O_3 are comparable; in all other specimens (runs A18-21) α-Fe_2O_3 occurs to a greater extent than Fe_3O_4. In no case did the amount of oxide exceed the amount of graphite, though in runs A21 IIe and III the amounts are comparable. The diffraction pattern from segments VI of run A19a (below the travel of the top ring) showed only a few spots due to the presence of graphite. This is typical of patterns from unused ring and bore segments.

The following conclusions may be noted:

With the use of clear fuel and an oil additive (run A4) strong patterns of α-Fe_2O_3 and spinel type oxide (Fe_3O_4 or $ZnFe_2O_4$) occur at the top of the piston travel, these diminish down the length of the cylinder and finally disappear at the bottom. The graphite distribution is just the reverse. The amount of spinel type oxide is definitely larger than the amount of α-Fe_2O_3 on the cylinder segments.

With the use of clear fuel and no oil additives the distribution of graphite is like that of A4, moderate at the top, increasing

down the bore, but the predominant oxide pattern that characterized the top of the bore in run A4 is absent in runs A20 and A21; instead the amount of oxide is never greater than the amount of graphite and stays about the same from segment to segment. The α-Fe_2O_3 pattern is stronger than that of Fe_3O_4 in six of the eight cuts from A20 and A21.

In runs where leaded fuel was used (A2, A18, A19) the distribution of oxide was reversed with respect to run A4, where the strongest oxide was present at the top. The well defined patterns characteristic of predominant graphite were found on the top as well as the bottom on the cylinder bores in runs A18 and A19. α-Fe_2O_3 is stronger than Fe_3O_4 on all specimens.

There is no evidence of lead or lead compounds on any of the cylinder bores examined.

Runs with Iron Carbonyl Fuels: Ring Specimens. The runs with $Fe(CO)_5$ fuel additive can be divided into two categories, runs A11, A12, and A13 with about 2.5 ml. $Fe(CO)_5$ per gallon of fuel; and runs A14, and A16 with 2.7 ml. $Fe(CO)_5$ plus a zinc additive. The additive, zinc dibutyldithiocarbamate, was reported to have poor inductability qualities in the test engine when blended in isooctane (A14) or isooctane plus 1% kerosene (A16) and the amount which actually entered the combustion chamber was estimated at about 20% of that theoretically required to burn with all of the iron carbonyl to form $ZnFe_2O_4$.

The results on all ring specimens from runs A11 through A16 are given in Table IX, and a summary is included in Table IV. No cylinder specimens were furnished from any iron carbonyl runs.

The runs with $Fe(CO)_5$ only in the fuel show moderate graphite with weak oxide in the short run (A13), very strong oxide in the run with prolonged break-in (A12), and very strong random graphite in the long run (A11). The relative amounts of the two oxides, α-Fe_2O_3 and Fe_3O_4, have been estimated for A12 which gave the best oxide diffraction pattern observed on any of the specimens furnished for this investigation; here the amount of α-Fe_2O_3 exceeds that of Fe_3O_4 although the diffraction pattern of the latter is not weak. It would be interesting to know whether the excessive amount of oxide in this

short run comes from oxidation of the ring material or of the iron carbonyl additive.

Run A11 shows very large amounts of graphite with random orientation and an extreme weight loss; the high total wear evidently opened up many inclusions of graphite which was spread over the ring but without the smooth rubbing required for orienting the graphite flakes. The oxide on this ring may have been strong but in any event it was obscured by the excessive graphite. It is interesting that the presence of much graphite is not sufficient by itself to hold down the wear rate; in this case a highly abrasive condition between the top ring and the cylinder bore caused both high wear and the release of graphite. Information on instantaneous wear rates would be required to show definitely whether the release of graphite had any healing effect on the abrasive condition.

The runs (A14 and A16) with iron carbonyl plus zinc dibutyldithiocarbamate do not show well-characterized diffraction patterns, but it was still possible to identify graphite, α-Fe_2O_3, Fe_3O_4 and (after abrasion with emery) α-Fe. The relative amounts of the oxides can not be estimated in these poorly resolved patterns. Here there is the possibility of the zinc spinel, $ZnFe_2O_4$, but as explained in a previous section it can not be distinguished from Fe_3O_4. In all of the specimens the oxide is stronger than the graphite; by contrast the runs without the zinc additive (A13 and A11) show a much more rapid build-up of graphite.

Conclusions based on the summary in Table IV may be stated as follows:

With clear fuel light graphite and moderate oxide are found in the short run; the longer run shows more of both. When iron carbonyl is added to the fuel the principal phase (for runs with "normal" break-in) is graphite. The high total wear observed in these runs is associated with the opening of many graphite inclusions which are spread over the face of the ring but the presence of this graphite does not appear to reduce the wear rate (unless the wear occurs primarily during the break-in period). The addition of the zinc additive suppresses the formation of well-defined layers of either graphite or iron oxides.

IV. PRELIMINARY OBSERVATIONS ON REPLICAS

During the course of the diffraction work a few unsuccessful attempts were made to prepare collodion replicas of piston ring faces for examination in the electron microscope, but the collodion could not then be lifted without rupturing. Very recently new variations in separating collodion replicas from rough substrates have been successfully applied, and selected micrographs of replicas from a series of ring specimens are reproduced in Figure 4.

The replicas were shadow-cast with palladium (for increasing contrast in the micrographs) and also treated with a suspension of polystyrene latex spheres of known diameter (0.25μ), which appear as black circles in the prints.

Some of the prints show that the replicas carried away some of the surface layer from the piston ring. The identification of these deposits separated from the surface should be attempted by electron diffraction using transmission through the replica; this would require eliminating the shadow-casting step in order to avoid the palladium metal. Several of the prints also show wear marks on the ring faces.

The advantages of electron micrographs of collodion replicas from ring faces lie in the evident variations occurring between different areas on the same ring and in the better detail than is observed in optical micrographs. A correlation of the electron micrographs with the diffraction results would lead to an identification of the phases according to their appearance in the micrographs, and a subsequent survey of a ring face with collodion replicas would then provide detailed information on the distribution of various phases over the surface of the ring.

It also appears from these preliminary pictures that such micrographs showing details of the abrasive effects might help in determining the wear mechanism.

The preliminary observations shown here warrant further application of this technique to piston ring problems.

V. GENERAL CONCLUSIONS

The phases identified by electron diffraction in reflection from the faces of the top piston rings in the engine run tests described in Section II and listed in Table IV include graphite and two iron oxides (α-Fe_2O_3 and Fe_3O_4). The relative amounts of the oxides on ring specimens could be estimated only for run A11. On several rings abrasion with 3/0 emery paper (to expose underlying phases) lead to the observation of the α-Fe pattern. On one ring the pattern of ordinary rust (γ-$Fe_2O_3 \cdot H_2O$) was found, probably from poor protection against the atmosphere between disassembly of the engine and examination of the ring.

No lead or lead compounds were observed on any ring or bore surfaces although the patterns of thirty-one oxides, halides and sulfates were considered.

The reproducibility of the test runs in terms of the relative amounts of the phases observed in relation to the test conditions (running time, fuel/air ratio, fuel additive, engine speed) is probably poor. Only one pair of duplicate runs was made (A6 and A18), and these differ on the segments examined from the top ring in showing graphite much stronger than the iron oxides in A6 and the oxides stronger than graphite in A18. Such discrepancies may mean that variations in the wear process occur in spite of constant values reported for the four engine variables named above or that the lack of a detailed survey of the total area of the top ring surface leads to accidental variations in the results reported from selected areas. Three different segments from the same ring were given an electron diffraction examination in each case; and the variations observed were small enough that the results given in Table IV fairly represent the behavior of all the segments. A more thorough test of variation in phase identity and distribution around one piston ring ought to be made with electron micrographs of collodion replicas.

Some correlations are suggested by the present data. In all runs (without respect to fuel additive or engine speed) the relative amounts of iron oxides and graphite may bear some relation to total running time. In the six shorter runs ranging from fourteen to fifty-five hours oxides predominate over graphite except in the run at twenty-four hours. In the seven longer runs ranging from seventy-five to ninety-nine hours graphite is stronger in five of them; the two runs at eighty-one hours show nearly equal graphite and oxide for one and stronger oxide for the other.

A correlation between total oxide and total wear is suggested for the runs with clear and leaded fuels, but not including the iron carbonyl runs. With cautious estimates of the change in total oxide from one ring to another it appears that low oxide goes with low wear. Of the seven runs in this group the three with the least wear (4 to 26 mgm.) show weak oxide, the three with intermediate wear (37 to 52 mgm.) show medium oxide in two cases and weak in the third, while the run with highest wear (117 mgm.) shows medium strong oxide.

The use of iron carbonyl in two runs with "normal" break-in (12 hours) shows strong predominating graphite and high wear in contrast with the runs with no fuel or oil additive. The simultaneous use of the zinc additive either suppresses the formation of well-characterized deposits of graphite and oxides or obscures them; the dominant oxide noted in Table IV may in fact be the zinc spinel, $ZnFe_2O_4$.

The cylinder bores show the same phases observed above with variations in the relative amounts of graphite and oxides at different positions along the stroke of the piston. The higher oxide, Fe_2O_3, is stronger than Fe_3O_4 with both clear and leaded fuels with no oil additive.

The use of electron diffraction methods does provide information on the relative amounts of phases occurring on engine surfaces under various running conditions. The present data suggest more careful studies with respect to running time and observed wear. In particular, the observation of instantaneous wear rates during engine operation should indicate periods of particular interest for electron diffraction examination (e.g., the comparison of surfaces at high and low instantaneous wear rates). When these observations are supplemented by examination of collodion replicas at high magnification, major progress should be made in determining the mechanism of the wear processes.

Table I. Interplanar Spacings (d values) and Relative Intensities for α-Fe_2O_3 and Fe_3O_4 (A.S.T.M. Card File of X-Ray Diffraction Data)

α-Fe_2O_3		Fe_3O_4	
d,Å	I	d,Å	I
		4.85	6
3.70	50		
		2.97	28
2.71	100		
2.53	70	2.53	100
		2.42	11
2.35	10		
2.21	50		
2.08	10	2.10	32
1.85	80		
1.70	100	1.71	16
1.61	50	1.61	64
1.49	80	1.48	80
1.46	80		
1.42	10		
1.36	30		
1.32	70	1.32	6
1.27	70	1.279	2
1.23	30	1.21	5
1.19	30		
1.16	30		
1.14	70		
1.11	70	1.12	10
1.08	10	1.09	32

Table II. Interplanar Spacings (d values) and Relative Intensities for Fe_3O_4, $ZnFe_2O_4$ and $CdFe_2O_4$. (A.S.T.M. Card File of X-Ray Diffraction Data).

Fe_3O_4		$ZnFe_2O_4$		$CdFe_2O_4$	
d,Å	I	d,Å	I	d,Å	I
4.85	6	4.84	20		
2.97	28	2.98	50	3.065	60
2.53	100	2.53	100	2.61	100
2.42	11	2.43	10	2.505	10
2.10	32	2.10	40	2.17	10
1.71	16	1.72	40	1.77	40
1.61	64	1.62	70	1.67	60
1.48	80	1.49	80	1.53	60
1.32	6	1.33	20	1.37	20
1.279	2	1.28	40	1.37	20
		1.27			
1.21	5	1.21		1.16	30
1.12	10	1.12	30	1.13	50

Table III. Lead Compounds With Available Diffraction Patterns

Pb	$2PbO \cdot PbCl_2$	$7PbO \cdot PbBr_2 \cdot 7H_2O$
Pb_2O	$PbO \cdot PbCl_2$ N form	$3PbO \cdot PbBr_2 \cdot H_2O$ A form
PbO (red)	2PbO•PbClBr	$3PbO \cdot PbBr_2 \cdot H_2O$ B form
PbO (yellow)	PbO•PbClBr N form	$PbO \cdot PbBr_2 \cdot H_2O$
Pb_3O_4	PbO•PbClBr R form	$7PbO \cdot PbBr_2 \cdot SiO_2$
Pb_5O_7	$7PbO \cdot PbBr_2$ Q form	$PbSO_4$
Pb_2O_3	$7PbO \cdot PbBr_2$ T form	$PbO \cdot PbSO_4$
Pb_5O_8	$2PbO \cdot PbBr_2$	$4PbO \cdot PbSO_4$
$2PbO \cdot PbCO_3$	$PbO \cdot PbBr_2$ L form	
$PbO \cdot PbCO_3$	$PbO \cdot PbBr_2$ N form	
$PbO \cdot 2PbCO_3$	$PbO \cdot PbBr_2$ R form	
$2PbCO_3 \cdot PbO \cdot H_2O$	$7PbO \cdot PbBr_2 \cdot 5H_2O$	

Table IV. Summary of Specimens and Results on Top Rings

Test Run	Fuel Additive[1] (ml/gal.)	Running Time[4] (hours)	Speed (rpm.)	F/A Ratio[5]	Total Weight Loss (mgm.)	No. of Exposures	Phases Observed[6] C(gr)	Phases Observed[6] α-Fe_2O_3 + Fe_3O_4
A0		0 + 0				6	w*	
A4	None[2]	12 + 73	1800	0.08		10	s*	w
A20	None	12 + 4	3600	"	4	15	w*	mw
A21	"	12 + 69	"	"	37	15	m*	m
A5	2.9 TEL(neat)	12 + 63	1800	0.06-0.08	26	12	s	w**
A3	3.0 TEL(62-MIX)	12 + 87	"	0.08	44	10	s	w
A19	"	12 + 4	3600	"	117	17	m*	ms*
A6	"	12 + 74	"	"	23	8	s*	w
A18	"	12 + 69	"	"	52	19	w*	m
A12	2.5 $Fe(CO)_5$	23 + 4	1800	0.08	62	8	w	s
A13	"	12 + 12	"	"	127	13	ms*	w*
A11	2.4-2.8 $Fe(CO)_5$	12 + 80	"	"	792	10	vs	vw
A16	2.7 $Fe(CO)_5$ + zinc dibutyl-dithiocarbamate[3]	8 + 6	"	"	22	18	m*	ms*
A14	"	12 + 43	"	"	245	26	w**	ms*

Footnotes on page 21a following.

Footnotes to Table IV (page 21).

[1]The base fuel was technical grade isoctane, average sulfur content, 0.005%; the base oil was Std. Oil (Indiana) stock with added V. I. improver.

[2]The crankcase oil contained zinc dithiophosphate and barium sulfonate additives; 0.05% Zn, 0.13% Ba.

[3]Zinc dibutyldithiocarbamate was found to have poor inductibility qualities in the test engine when blended in isoctane (A14) or isoctane + 1% kerosene (A16). The amount which actually did enter the combustion chamber is estimated to have been approximately 20% of that theoretically required to burn with all of the iron carbonyl to form $ZnFe_2O_4$.

[4]Running time is shown for hours of break-in and hours at full throttle.

[5]At full throttle.

[6]C(gr) represents graphite; α-Fe_2O_3 + Fe_3O_4 represents a mixture of the iron oxides in proportions that cannot be reliably estimated on the ring specimens. The relative amounts of graphite and iron oxides are estimated as follows: w-weak, mw-medium weak, m-medium, ms-medium strong, s-strong.

* - indicates marked discontinuties in diffraction rings due to preferred orientation in the phase.

** - indicates the occurrence of only occasional diffraction spots due to a very small number of particles of the phase.

Table V. Comparison of Interplanar Spacings and Relative Intensities from Typical Mixed Oxide Pattern with Standard Patterns.

Oxide Pattern (Specimen A12c)		α-Fe_2O_3 (electron diffraction standard)		Fe_3O_4 (A.S.T.M.)		Graphite (electron diffraction standard)	
d,Å	I	d,Å	I	d,Å	I	d,Å	I
		3.80	m				
						3.40	ms
2.97	mw			2.97	28		
2.71	m	2.73	s				
2.54	s	2.55	m	2.53	100		
		(2.35	w)	2.41	11		
2.25	w	2.23	ms				
2.13	ms					2.15	s
2.08	m	2.08	w	2.10	32	2.06	m
2.03	m					2.03	m
1.94	w					1.96	(vw)
1.86	m	1.85	ms				
						1.80	vw
1.72	ms	1.70	s	1.71	16		
						1.66	vw
1.62	ms	1.61	ms	1.61	80	(1.63	vw)
1.50	s	1.49	ms	1.48	80	1.52	vw
1.47	s	1.46	ms				
		(1.42	vw)				
		(1.36	w)			1.34	vw
1.31	m	1.31	s	1.32	6	(1.31	vw)
		(1.27	m)	1.279	20		
1.23	s	(1.23	w)	1.21	5	1.23	s
1.16	s	1.16	w			1.15	s
				1.12	10		

Table VI. Phases Observed on Top Ring Faces From Runs with Clear Fuel

Ring Segment	Fuel Additives (ml/gal)	Total Running Time (hours)	Speed (rpm)	Phases		
				Graphite	α-Fe_2O_3 + Fe_3O_4	α-Fe
A4a	None[1]	12 + 73	1800	s*	vw	
A4c[2]	None	"	"	ms	w	m
A4e[2]	"	"	"	ms		m
A20a	None	12 + 4	3600	w*	mw	
A20c	"	"	"	ms*	mw	
A21a	None	12 + 69	3600	m*	m	
A21c	"	"	"	m*	m	
A21e	"	"	"	ms*	m	

[1] Zinc dithiophosphate and barium sulfonate oil additives

[2] Abraded with 3/0 emery

* - marked discontinuities in diffraction rings

Table VII. Phases Observed on Top Ring Faces From Runs with Leaded Fuels

Ring Segment	Fuel Additives (ml/gal)	Total Running Time (hours)	Speed (rpm)	Phases: Graphite	Phases: α-Fe_2O_3 + Fe_3O_4	Phases: Other
A5a	2.9 TEL(neat)	12 + 63	1800	s	w**	
A5c	"	"	"	w		s[2]
A5e	"	"	"	s*		
A5e[1]	"	"	"	s		m(α-Fe)
A3	3.0 TEL(62-MIX)	12 + 87	1800	s	w	
A19c	3.0 TEL(62-MIX)	12 + 4	3600	mw*	ms*	
A19e	"	"	"	m*	ms*	
A6a	3.0 TEL(62-MIX)	12 + 74	3600	vs*	vw	
A6c[1]	"	"	"	s	w**	m(α-Fe)
A6e	"	"	"	s*	w	
A18a	3.0 TEL(62-MIX)	12 + 69	3600	w*	m	
A18e	"	"	"	vw*	m	

[1] Abraded with 3/0 emery

[2] s(γ-$Fe_2O_3 \cdot H_2O$)

* - marked discontinuities in diffraction rings

** - diffraction rings indicated only by occasional spots

Table VIII. Phases Observed on Segments of Cylinder Bores

Segment		Fuel Additives (ml/gal)	Total Running Time (hours)	Speed (rpm)	Phases: Graphite	Phases: α-Fe_2O_3 + Fe_3O_4	Phases: Other
A 4e	II	None[1]	12 + 73	1800	m*	s*	
	III	"	"	"	m*	s*	
	IV	"	"	"	ms*	mw*	
	V	"	"	"	s*	w*	
A 20a	II	None	12 + 4	3600	ms	w	
	III	"	"	"	mw**	mw**	
	IV	"	"	"	mw**	mw**	
	V	"	"	"	s	mw	
A 21e	II	None	12 + 69	3600	m	m	
	III	"	"	"	m	m	
	IV	"	"	"	s	w**	
	V	"	"	"	ms	m	
A 5g	II[2]	2.9 TEL(neat)	12 + 63	1800	s		m*[3]
	III	"	"	"	w		s
	IV	"	"	"	m*		w**
	V	"	"	"	s*		w**
A 2e	I	3.0 TEL(62-MIX)	12 + 108	1800	s*	w**	
	II	"	"	"	s*	w**	
	III	"	"	"	w	ms	
	IV	"	"	"	mw	w	
	V	"	"	"	mw		
A 18a	II	3.0 TEL(62-MIX)	12 + 69	3600	s*	w*	
	III	"	"	"	mw*	mw*	
	IV	"	"	"	mw*	mw*	
	V	"	"	"	s	m	
A 19a	II	3.0 TEL(62-MIX)	12 + 4	3600	s	w	
	III	"	"	"	s	m	
	IV	"	"	"	s	mw	
	V	"	"	"	s	m	
	VI	"	"	"	w**		

[1] Zinc dithiophosphate and barium sulfonate oil additives

[2] Abraded with 3/0 emery

[3] All cuts from segment A5g show γ-$Fe_2O_3 \cdot H_2O$; the abraded specimen A5gII also shows α-Fe.

* - marked discontinuities in diffraction rings
**- diffraction rings indicated only by occasional spots

Table IX. Phases Observed on Top Ring Faces from Runs with Iron Carbonyl Fuels

Ring Segment	Fuel Additives (ml/gal)	Total Running Time (hours)	Speed (rpm)	Phases		
				Graphite	α-Fe	α-Fe_2O_3 + Fe_3O_4
A12a	2.5 $Fe(CO)_5$	23 + 4	1800	vw		vs
A12c	"	"	"	w		s
A12e[1]	"	"	"	s	s	w
A13a	2.5 $Fe(CO)_5$	12 + 12	1800	mw*		mw*
A13a[1]	"	"	"	s	s	w*
A13c	"	"	"	s*		vw*
A13e	"	"	"	ms*		w*
A11c	2.4-2.8 $Fe(CO)_5$	12 + 80	1800	vs		vw
A11e	"	"	"	vs		vw
A16a	2.7 $Fe(CO)_5$ + zinc add.	8 + 6	1800	w**		mw*
A16a[1]	"	"	"	s	m	mw*
A16c	"	"	"	m*		ms*
A16e	"	"	"	m*		s*
A14a	2.7 $Fe(CO)_5$ + zinc add.	12 + 43	1800	vw**		s*
A14c	"	"	"	w*		mw*
A14e	"	"	"	w**		ms*

[1] Abraded with 3/0 emery.

* - marked discontinuities in diffraction rings
**- diffraction rings indicated only by occasional spots

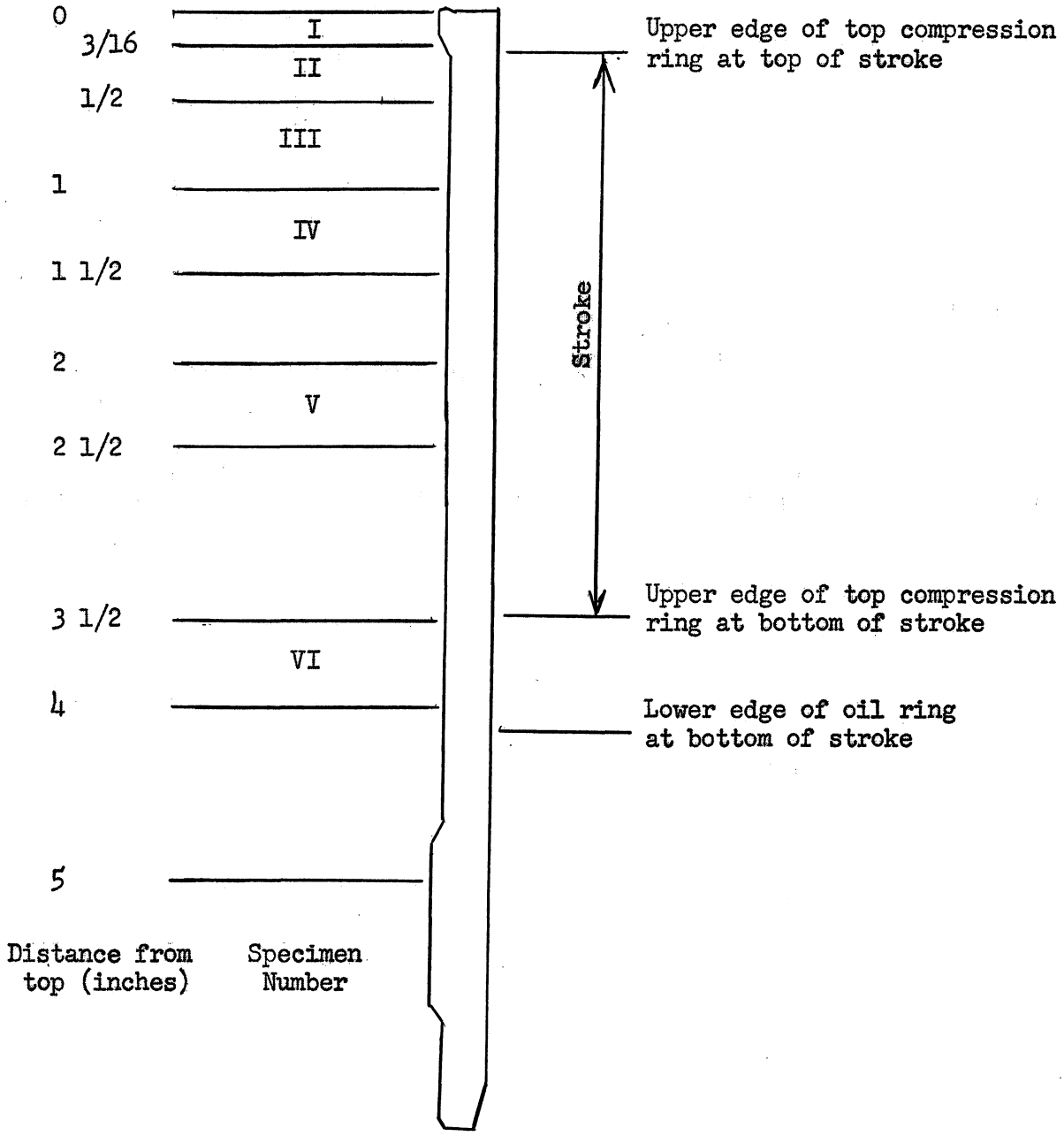

Figure 1. Location of Specimens cut from Cylinder Bores

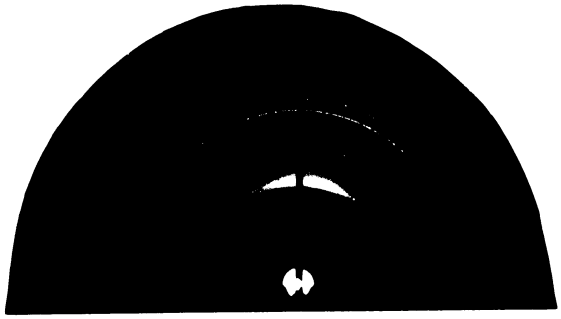

a. Graphite

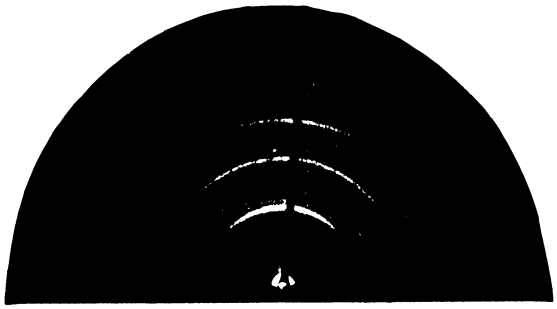

b. α-Fe_2O_3

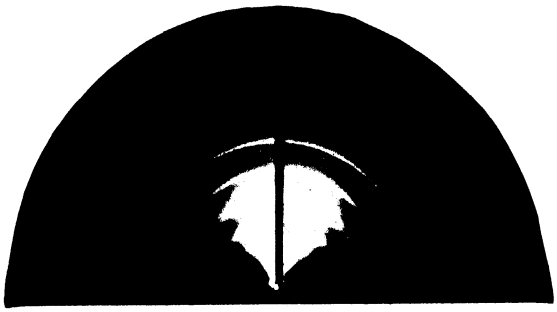

c. γ-$Fe_2O_3 \cdot H_2O$

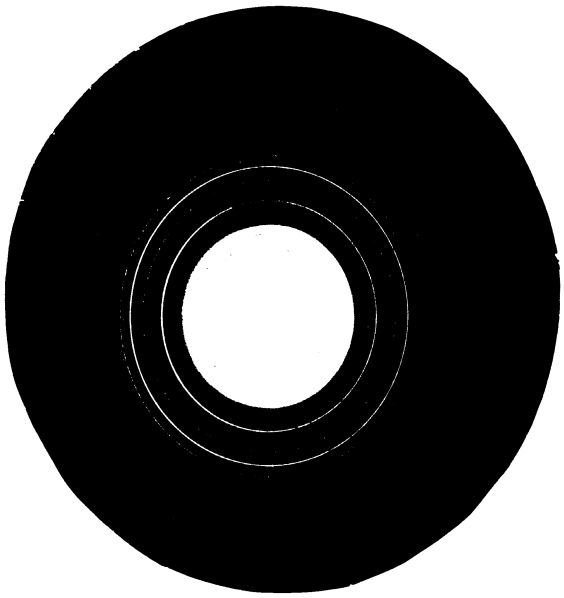

d. ZnO

Figure 2. Standard Electron Diffraction Patterns

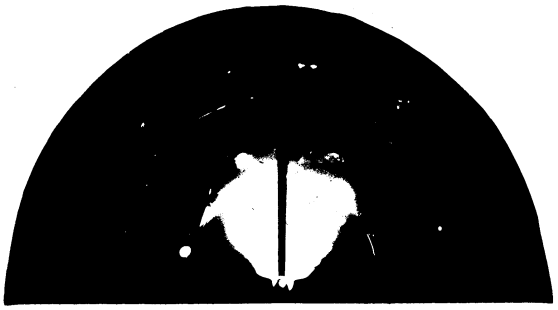

a. New ring showing occasional graphite

b. Used ring, showing graphite (nearly random) + weak oxide

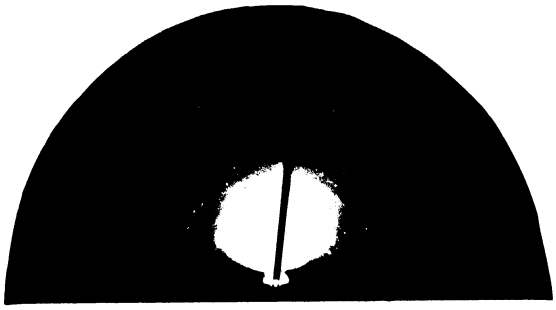

c. Used ring, showing strong α-Fe_2O_3 + Fe_3O_4

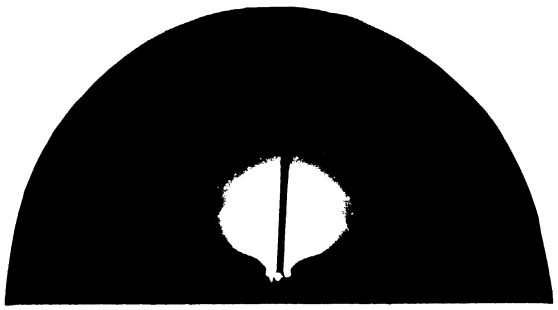

d. Used bore, showing α-Fe_2O_3 + Fe_3O_4

Figure 3. Electron Diffraction Patterns from Ring and Bore Specimens

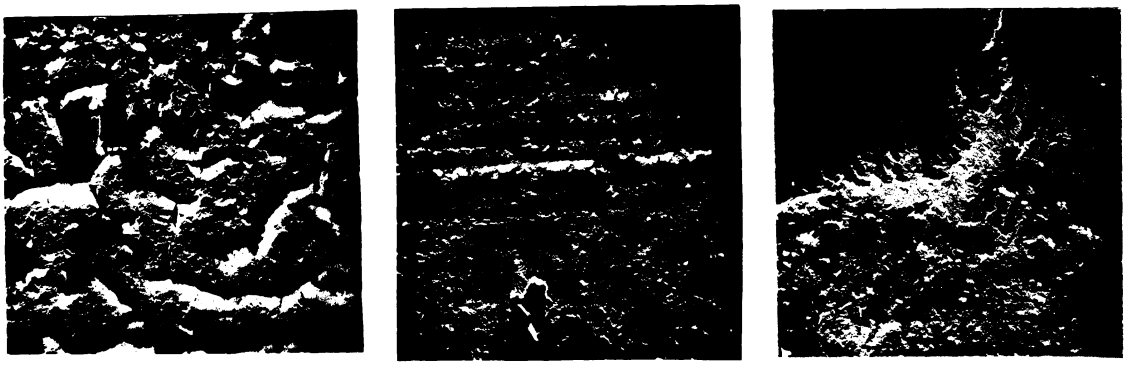

a. Top Ring Segment A12a

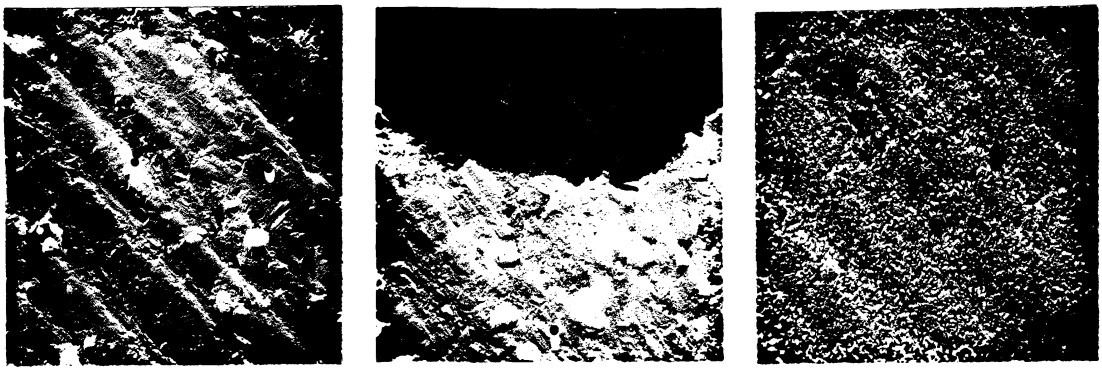

b. Top Ring Segment A14a

c. Top Ring Segment A18e

Figure 4. Electron Micrographs of Collodion Replicas of Ring Faces 4000X (except c-1 at 10000X)